

Supporting Information

Stimuli-Responsive Luminescent Bis-Tridentate Ru(II) Complexes toward the Design of Functional Materials

Manoranjan Bar, Sourav Deb, Animesh Paul and Sujoy Baitalik*

Department of Chemistry, Inorganic Chemistry Section, Jadavpur University,
Kolkata 700032, India

Physical Measurements. UV-vis absorption spectra were recorded using a Shimadzu UV 1800 spectrometer. Steady state luminescence spectra were acquired either by a Perkin–Elmer LS55 or a Horiba Fluoromax-4 spectrofluorometer. Luminescence quantum yields were determined using literature method taking $[\text{Ru}(\text{bpy})_3]^{2+}$ as the standard. Luminescence lifetime measurements were carried out by using time-correlated single photon counting set up from Horiba Jobin-Yvon. The samples were excited with 450 nm Nanoled. The luminescence decay data were collected on a Hamamatsu MCP photomultiplier (R3809) and were analyzed by using IBH DAS6 software. ESI mass spectra were recorded on a Waters Xevo G2 QTOF mass spectrometer. NMR spectra of the compounds were acquired on either Bruker 400 or 500 MHz spectrometer.

The electrochemical measurements were carried out with a BAS epsilon electrochemistry system. A three–electrode assembly comprising a Pt (for oxidation) or glassy carbon (for reduction) working electrode, Pt auxiliary electrode, and Ag/AgCl reference electrode were used. The square wave voltammetric (SWV) measurements were carried out at 25°C in acetonitrile solution of the complexes (*ca.* 1 mM) and the concentration of the supporting electrolyte (TEAP) was maintained at 0.1 M. All of the potentials reported in this study were referenced against the Ag/AgCl electrode, which under the given experimental conditions gave a value of 0.36 V for the ferrocene/ferrocenium couple.

The sensing studies of the receptors with different anions and cations were carried out in acetonitrile as well as in water medium. Tetrabutylammonium (TBA) salts of different anions and hydrated perchlorate salts of the metals were used for titration experiments. The binding/equilibrium constant towards the ions were evaluated from the absorbance data using equation (1).

$$A_{\text{obs}} = (A_0 + A_{\infty}K[\text{G}]_{\text{T}})/(1 + K[\text{G}]_{\text{T}}) \quad (1)$$

where A_{obs} is the observed absorbance, A_0 is the absorbance of the free receptor, A_{∞} is the maximum absorbance induced by the presence of a given ionic guest, $[\text{G}]_{\text{T}}$ is the total concentration of the guest, and K is the binding/equilibrium constant of the host–guest entity. Binding constants were performed in duplicate, and the average value is reported.

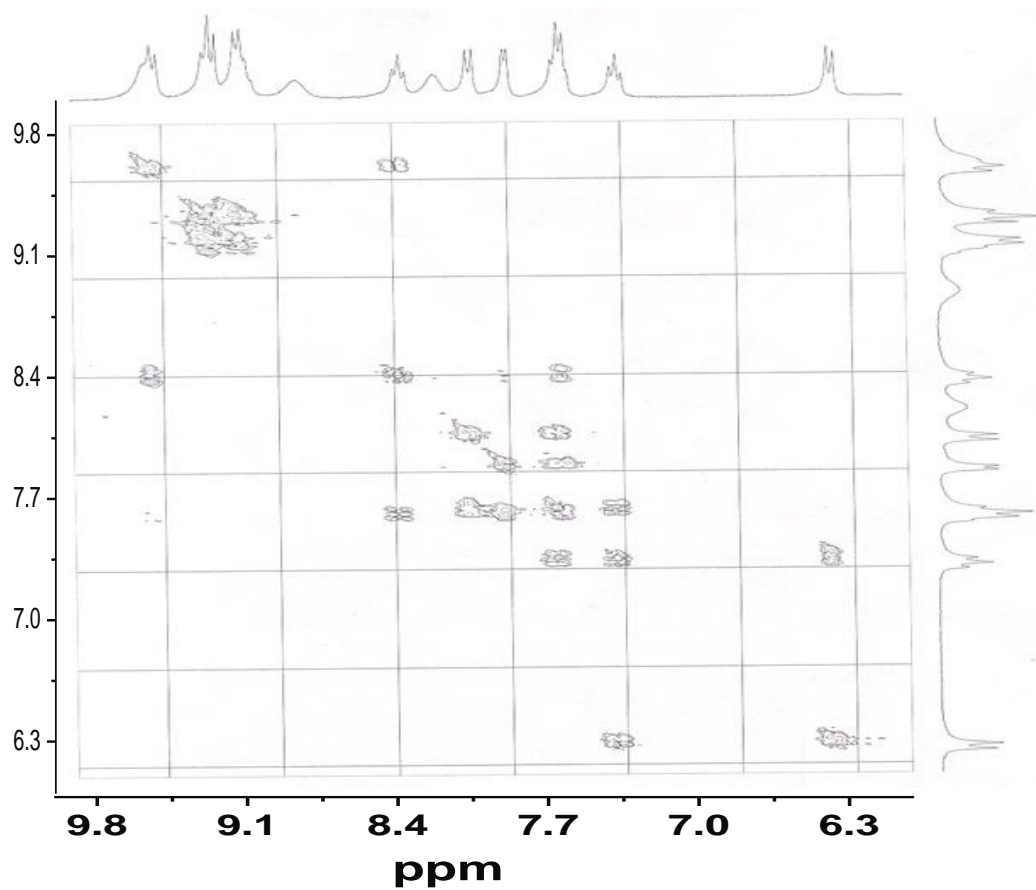


Figure S2. (¹H-¹H) COSY NMR spectrum of [(dipy-Hbzim-tpy)Ru(H₂pbbzim)](ClO₄)₂ (**2**) in DMSO-*d*₆.

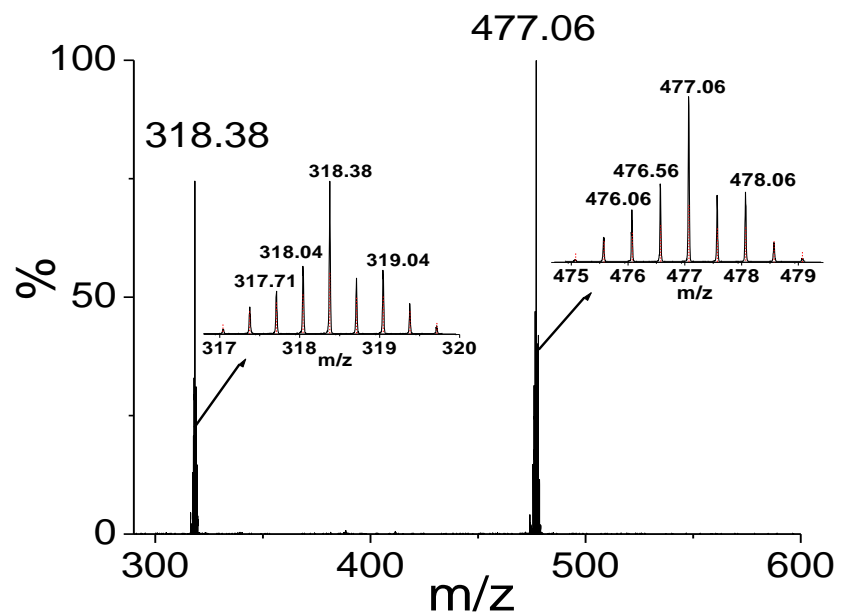


Figure S3. ESI-MS (positive) for the cation of **1**, $[(\text{dipy-Hbzim-tpy+H})\text{Ru}(\text{tpy-PhCH}_3)]^{3+}$ ($m/z = 318.38$) and $[(\text{dipy-Hbzim-tpy})\text{Ru}(\text{tpy-PhCH}_3)]^{2+}$ ($m/z = 477.06$) in MeCN showing the observed and simulated isotopic distribution patterns.

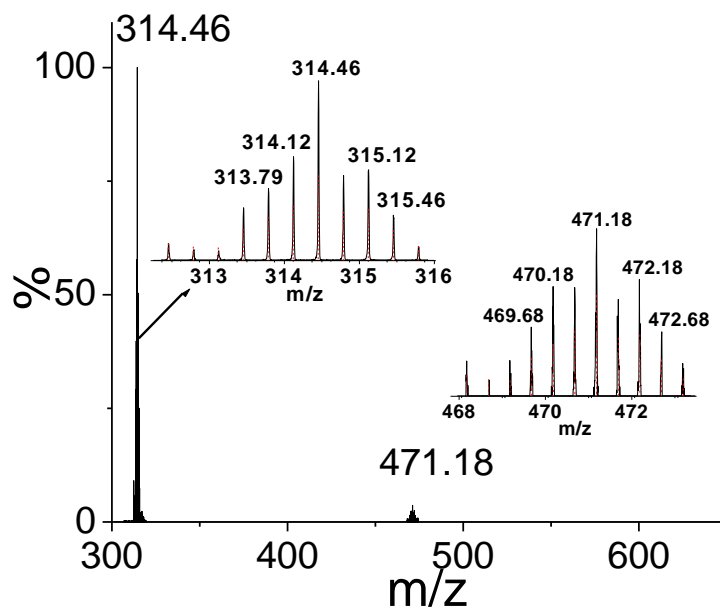


Figure S4. ESI-MS (positive) for the complex cation of **2**, [(dipy-Hbzim-tpy+H)Ru(H₂pbbzim)]³⁺ ($m/z = 314.46$) and [(dipy-Hbzim-tpy)Ru(H₂pbbzim)]²⁺ ($m/z = 471.18$) in MeCN showing the observed and simulated isotopic distribution patterns.

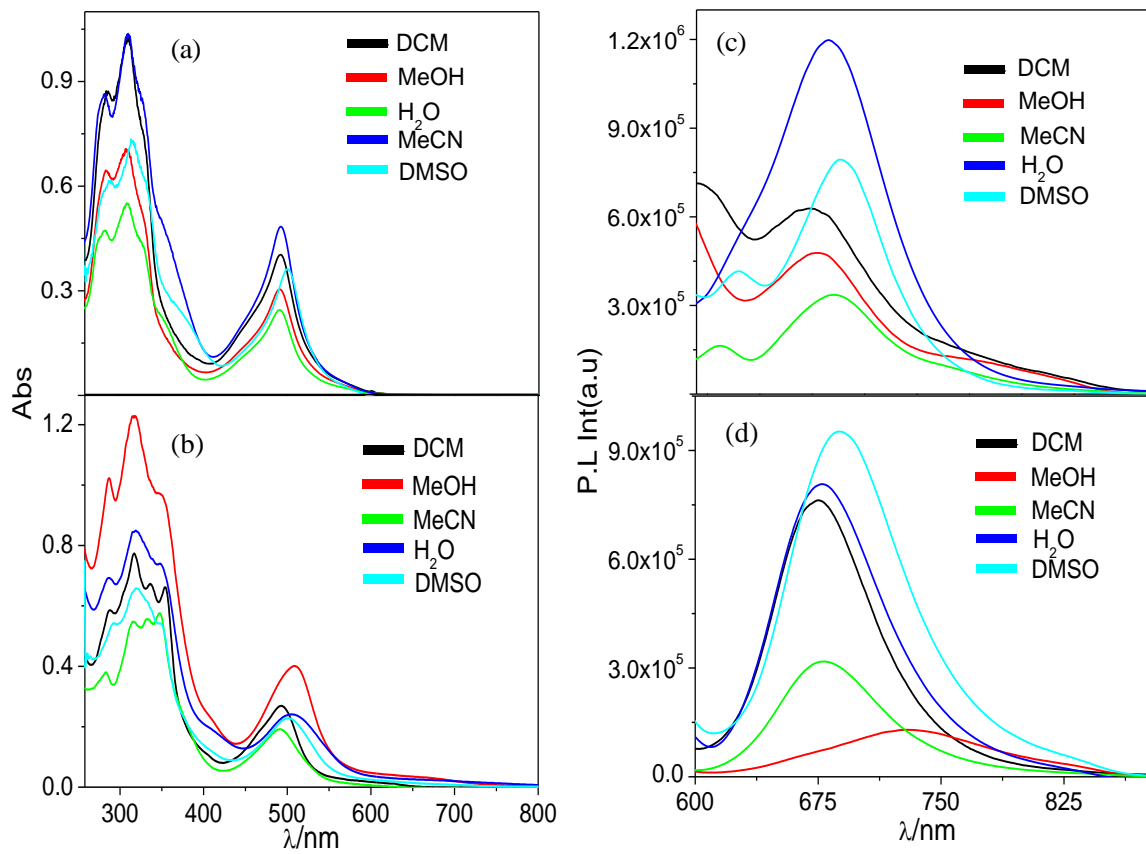


Figure S5. Absorption and emission ($\lambda_{\text{ex}} = 490 \text{ nm}$) spectra of **1** (a and c, respectively) and **2** (b and d, respectively) in few solvents.

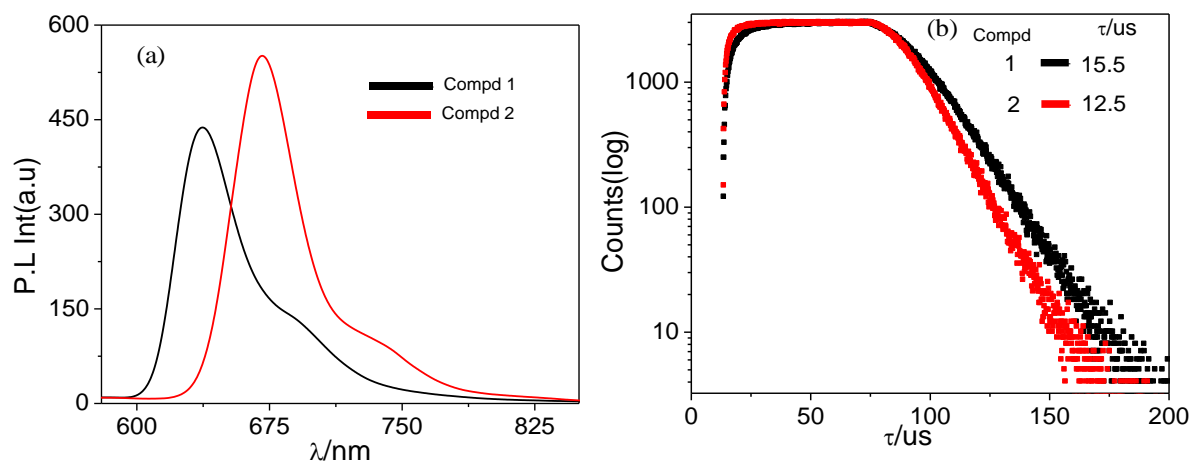


Figure S6. Luminescence ($\lambda_{\text{ex}} = 490 \text{ nm}$) decays and lifetime ($\lambda_{\text{ex}} = 450 \text{ nm}$) of the complexes in EtOH-MeOH (4:1, v/v) at 77K.

Electrochemical data for **1** and **2** in MeCN.

Compds	Oxidation $E_{1/2}(\text{ox}), \text{V}$	Reduction $E_{1/2}(\text{red}), \text{V}$
1	1.3	-0.88, -1.12, -1.50, -1.88
2	1.0	-1.09, -1.43, -1.57, -2.09

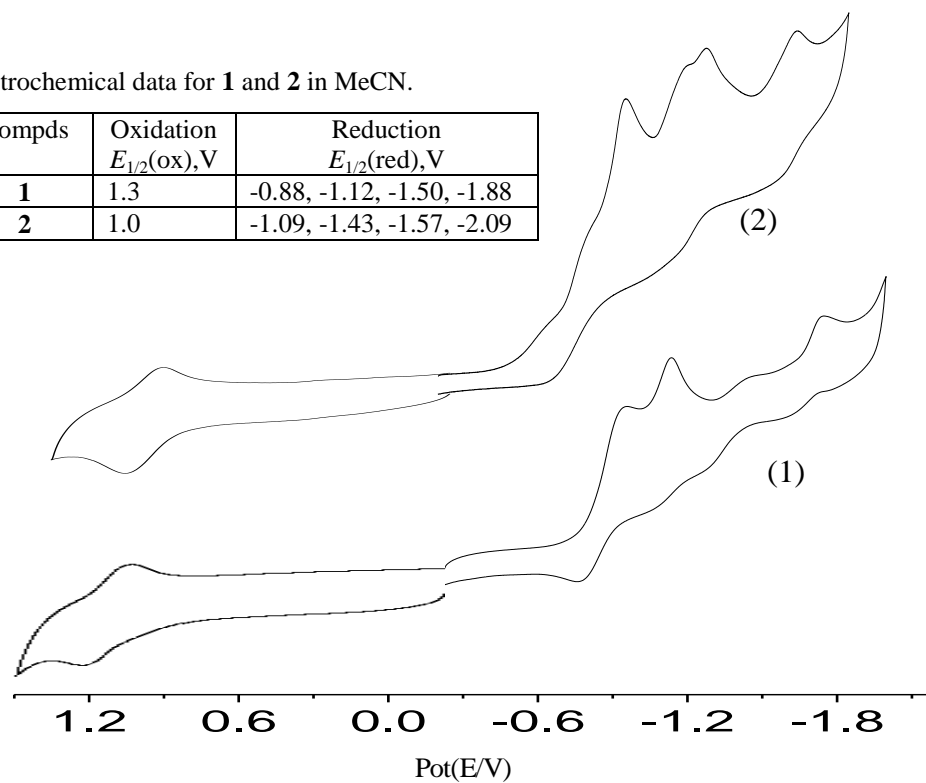


Figure S7. CVs of the complexes in MeCN using Pt as the working electrode and Ag/AgCl as the reference electrode. The scan rate is 100mVs^{-1} .

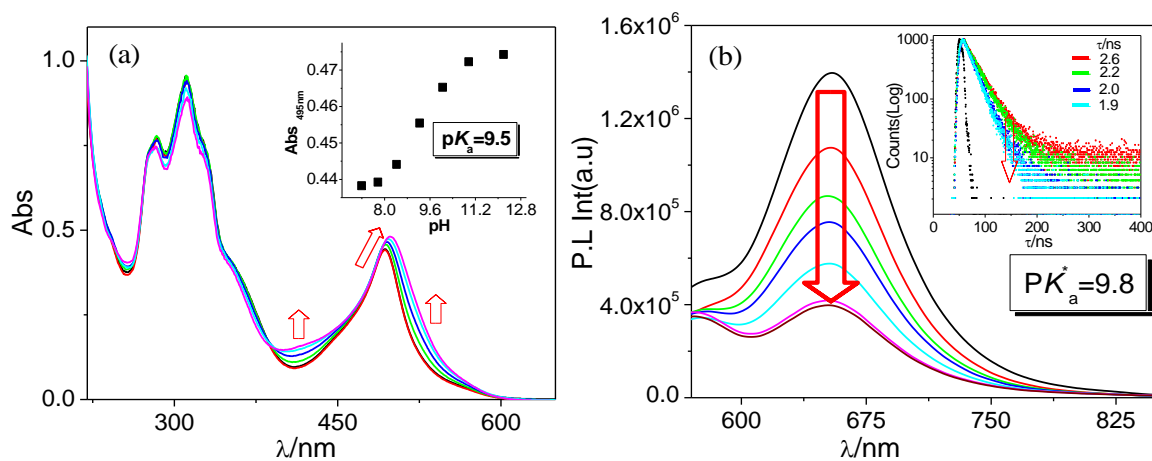


Figure S8. Absorption (a) and emission ($\lambda_{\text{ex}} = 490 \text{ nm}$) (b) spectral changes of **1** as a function of pH in water. The inset of figure a shows the change of absorbance, while inset of figure b indicates the change of lifetime with pH.

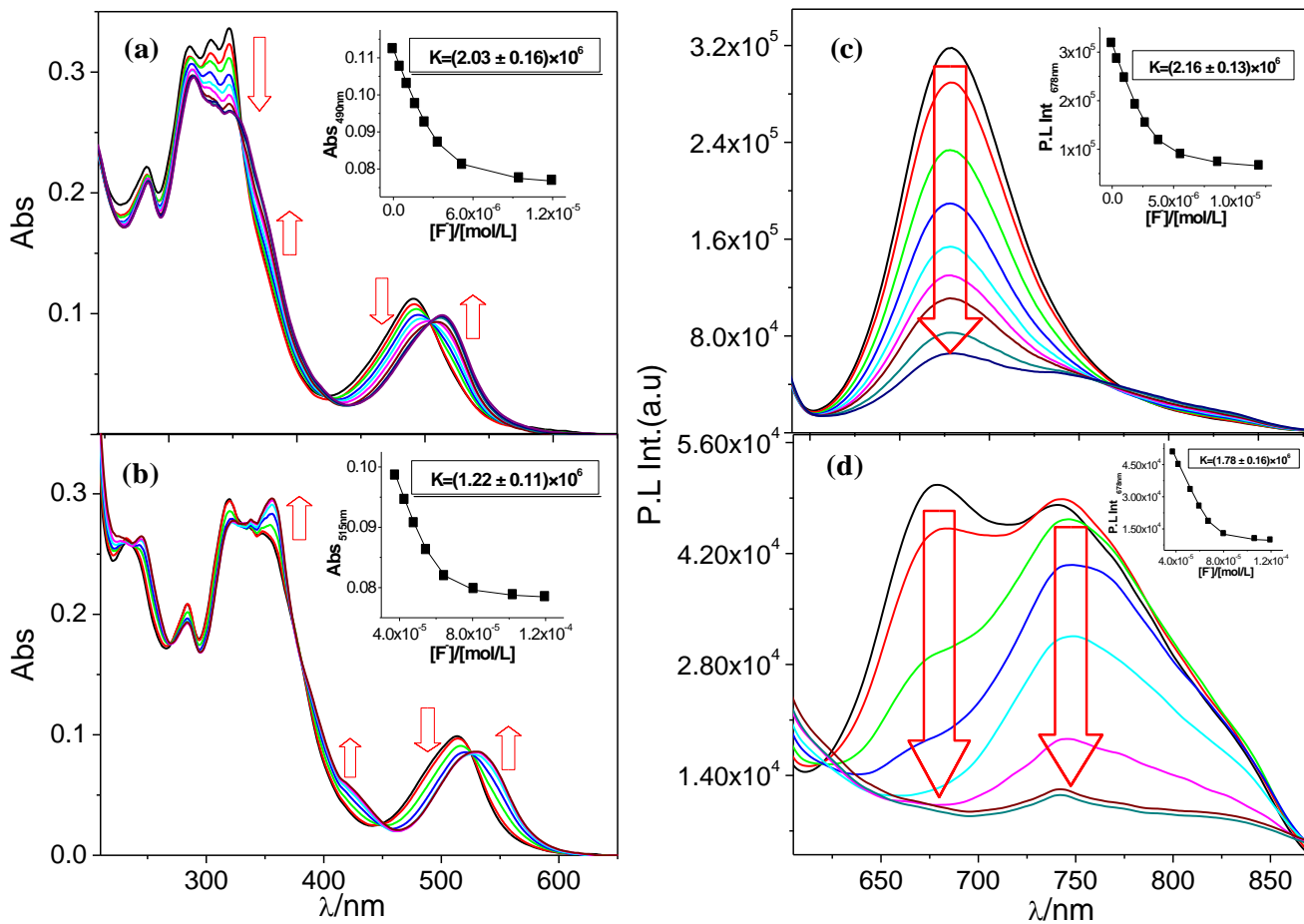


Figure S9. UV-vis absorption (a and b) and emission ($\lambda_{ex} = 490$ nm) (c and d) spectral changes of **2** in MeCN upon addition of F^- . The insets show the fit of the experimental absorbance and luminescence data to a 1:1 binding profile.

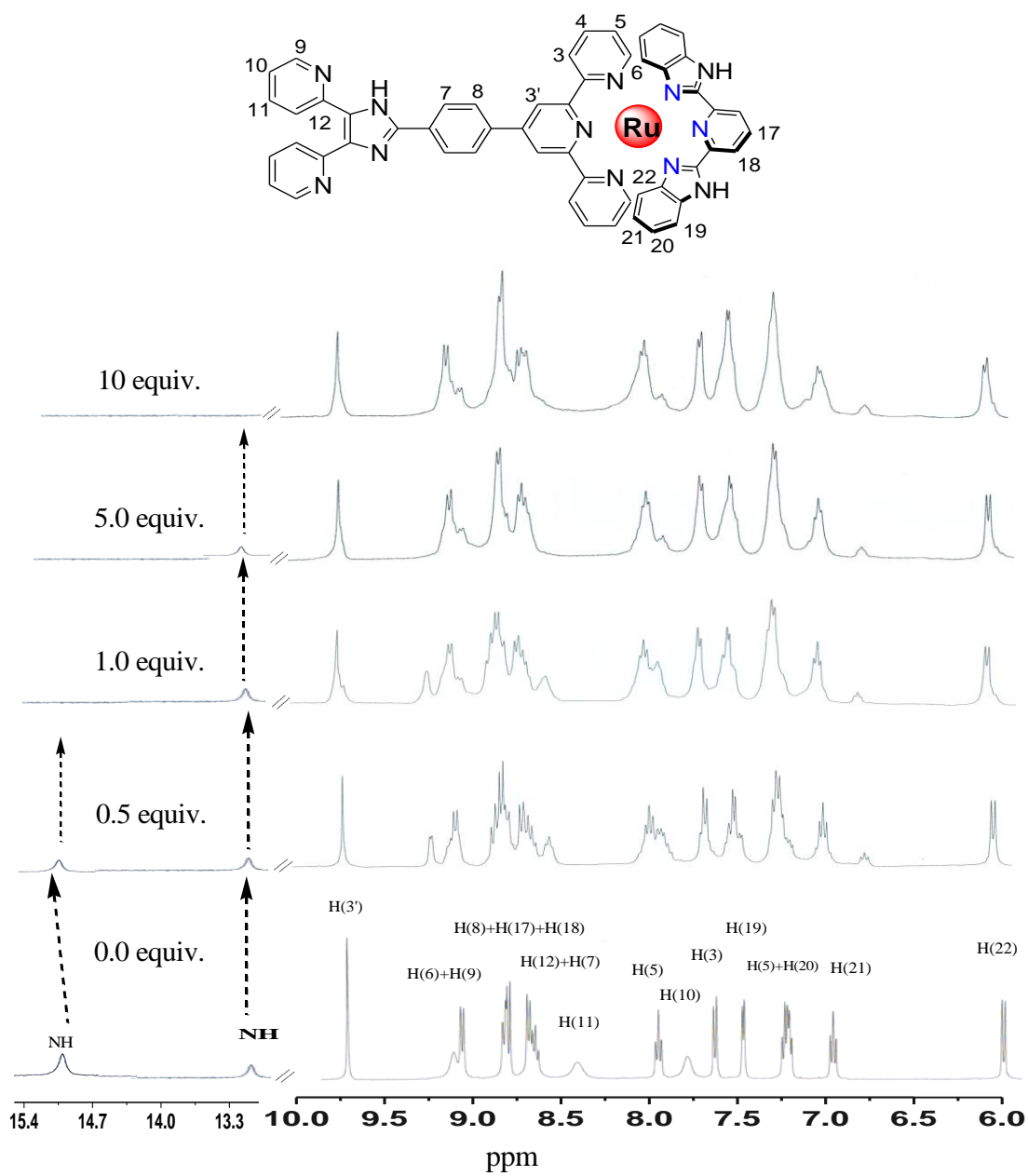


Figure S10. ^1H NMR titration profile of **2** in $\text{DMSO}-d_6$ upon incremental addition of H_2PO_4^- ion.

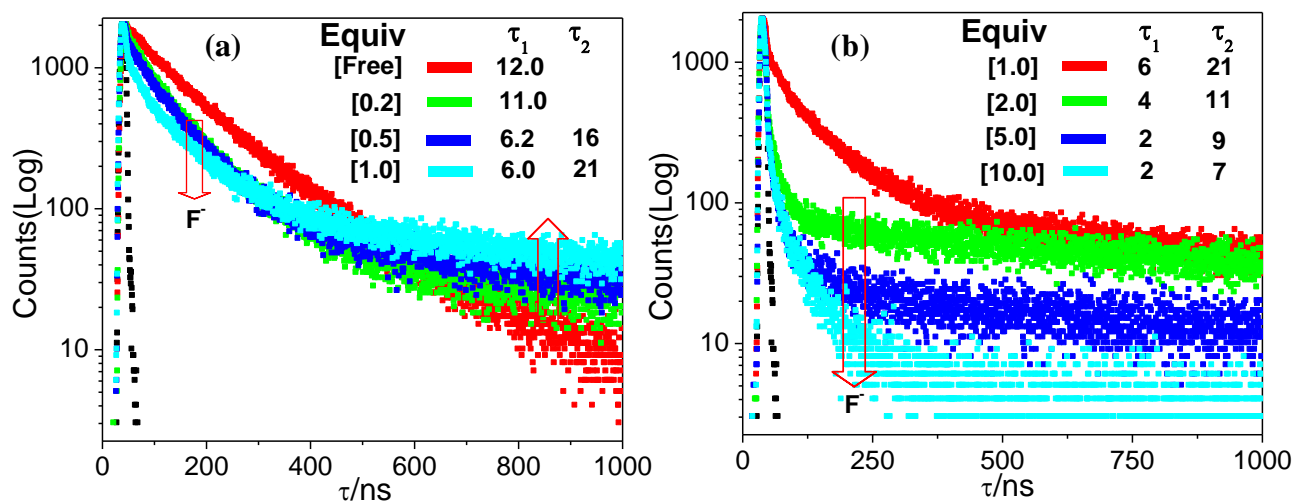


Figure S11. Change in time-resolved luminescence decay ($\lambda_{ex} = 450$ nm) of **2** (a and b) in MeCN at room temperature upon incremental addition of F^- . Insets show the lifetimes of the complex.

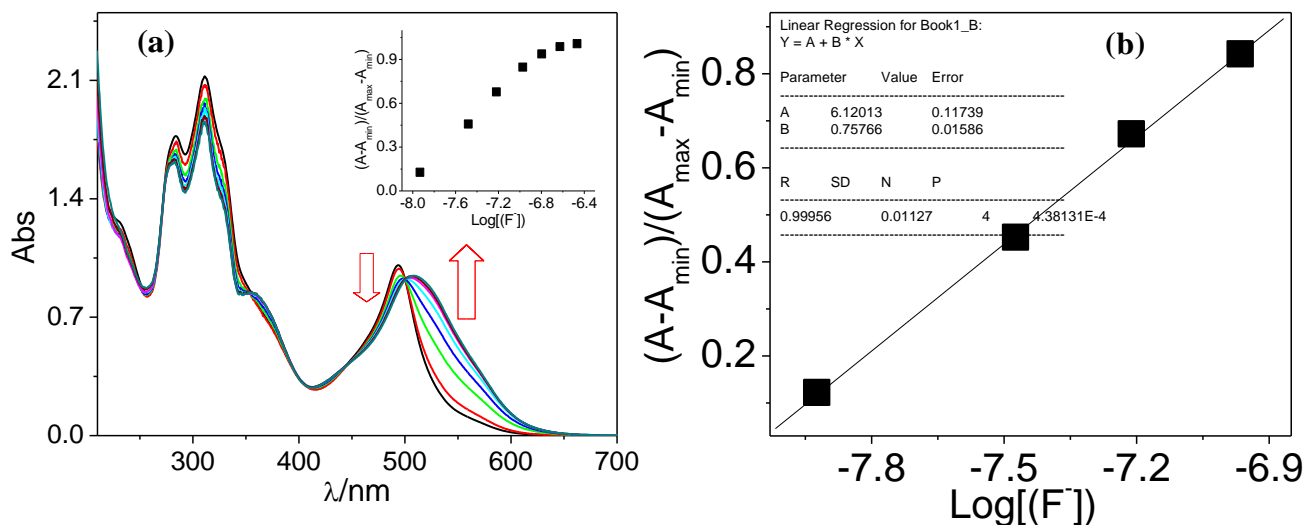


Figure S12. (a) Absorption spectral changes during the titration of the receptor **1** (1.0×10^{-5} M) with F^- in MeCN medium, inset: Normalized absorbance between the minimum absorbance and the maximum absorbance. (b) A plot of $(A-A_{min})/(A_{max}-A_{min})$ vs $\text{Log}([F^-])$, the calculated detection limit of receptor is 9.9×10^{-9} M.

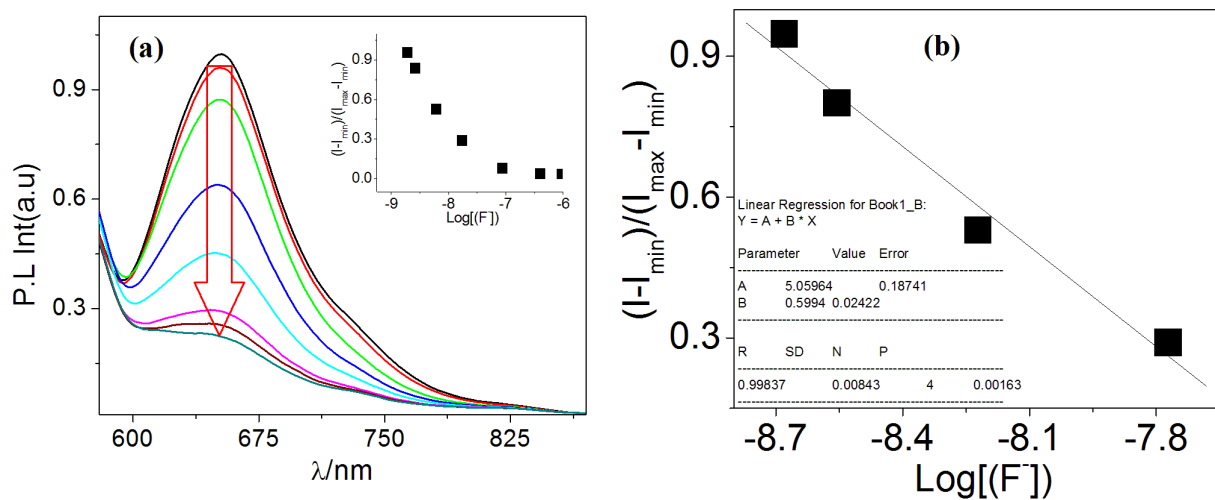


Figure S13. (a) Emission ($\lambda_{\text{ex}} = 490 \text{ nm}$) spectral changes during the titration of the receptor **1** ($1.0 \times 10^{-5} \text{ M}$) with F^- in MeCN medium, inset: Normalized intensity between the minimum intensity and the maximum intensity. (b) A plot of $(I-I_{\text{min}})/(I_{\text{max}}-I_{\text{min}})$ vs $\text{Log}([\text{F}^-])$, the calculated detection limit of receptor is $9.1 \times 10^{-9} \text{ M}$.

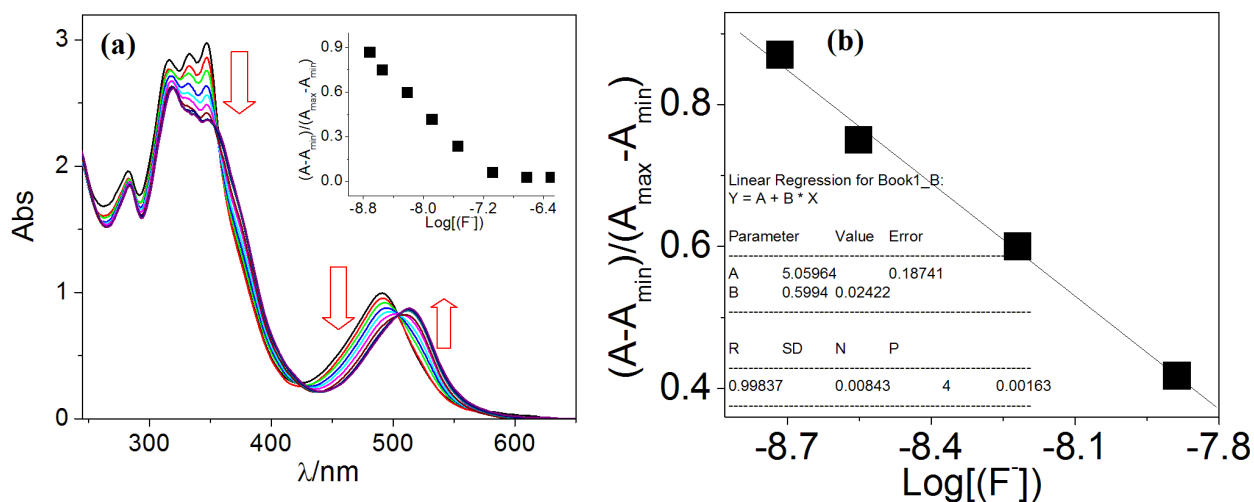


Figure S14. (a) Absorption spectral changes during the titration of the receptor **2** ($1.0 \times 10^{-5} \text{ M}$) with F^- in MeCN medium, inset: Normalized absorbance between the minimum absorbance and the maximum absorbance. (b) A plot of $(A-A_{\text{min}})/(A_{\text{max}}-A_{\text{min}})$ vs $\text{Log}([\text{F}^-])$, the calculated detection limit of receptor is $1.0 \times 10^{-9} \text{ M}$.

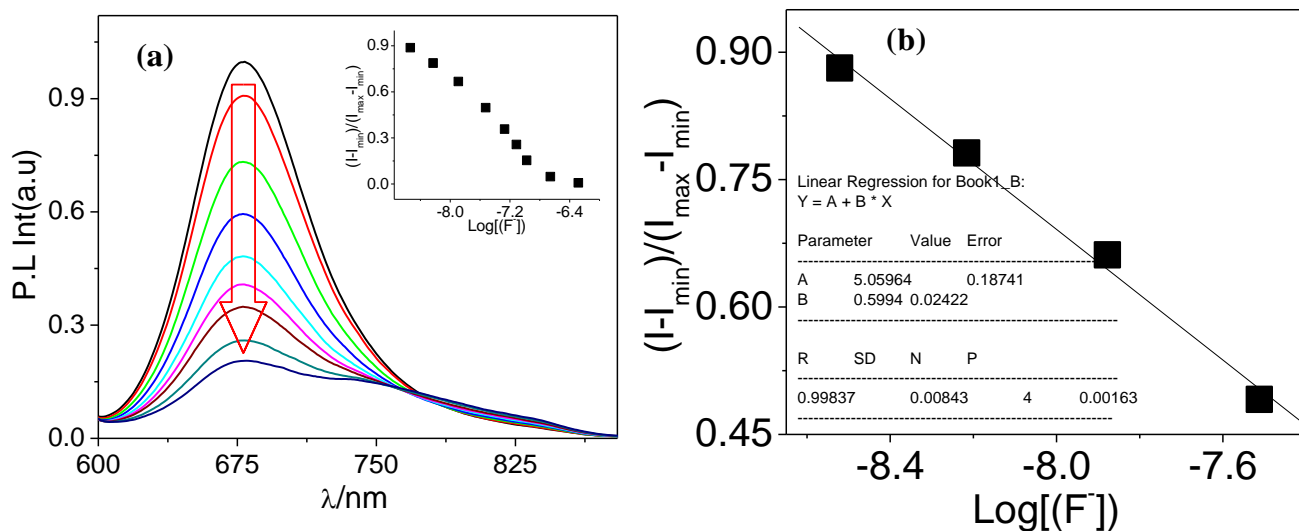


Figure S15. (a) Emission ($\lambda_{\text{ex}} = 490 \text{ nm}$) spectral changes during the titration of the receptor **2** ($1.0 \times 10^{-5} \text{ M}$) with F^- in MeCN medium, inset: Normalized intensity between the minimum intensity and the maximum intensity. (b) A plot of $(I-I_{\text{min}})/(I_{\text{max}}-I_{\text{min}})$ vs $\text{Log}([\text{F}^-])$, the calculated detection limit of receptor is $2.0 \times 10^{-9} \text{ M}$.

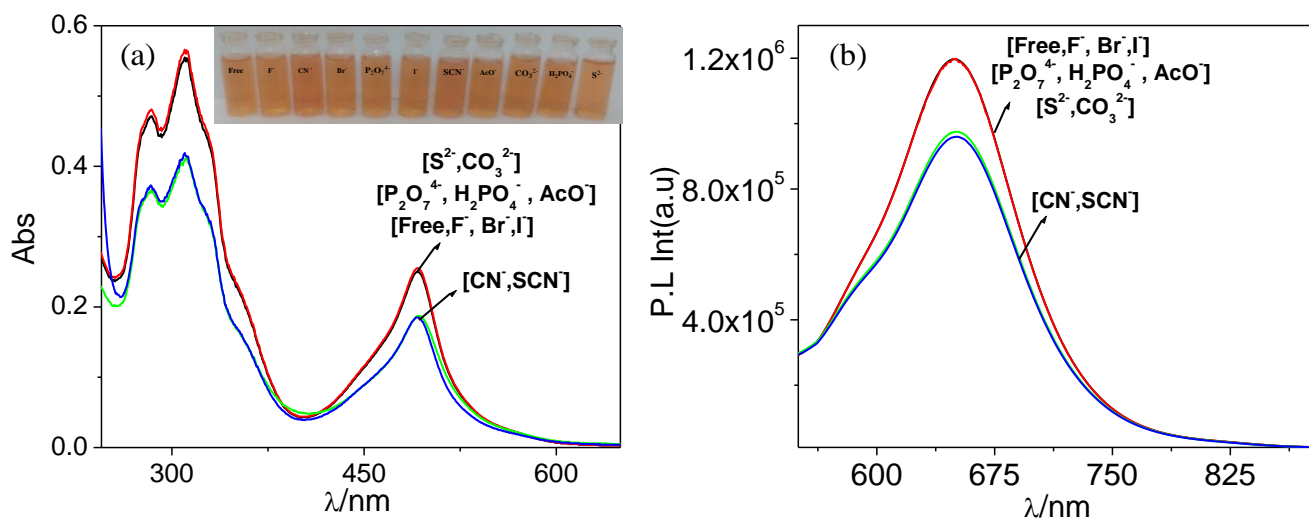


Figure S16. UV-vis absorption and emission ($\lambda_{\text{ex}} = 490 \text{ nm}$) spectral changes of **1** (a and b, respectively) in aqueous solution upon addition of different anions as their TBA salts. The visual color changes upon addition of different anions are shown in the insets of Figure (a).

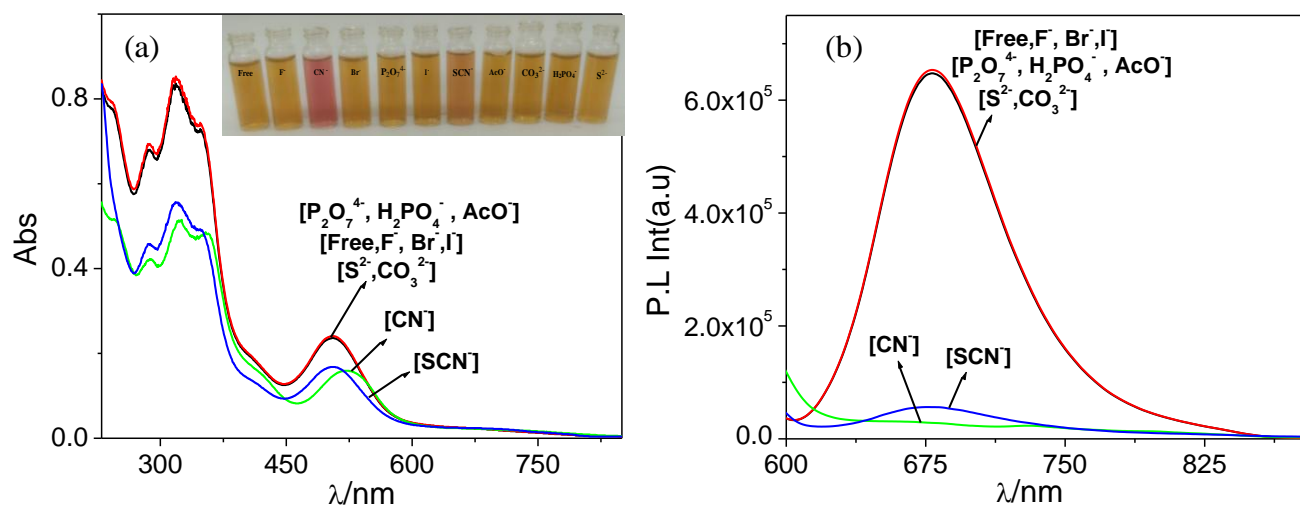


Figure S17. UV-vis absorption and emission ($\lambda_{\text{ex}} = 490 \text{ nm}$) spectral changes of **2** (a and b, respectively) in aqueous solution upon addition of different anions as their TBA salts. The visual color changes upon addition of different anions are shown in the insets of Fig (a).

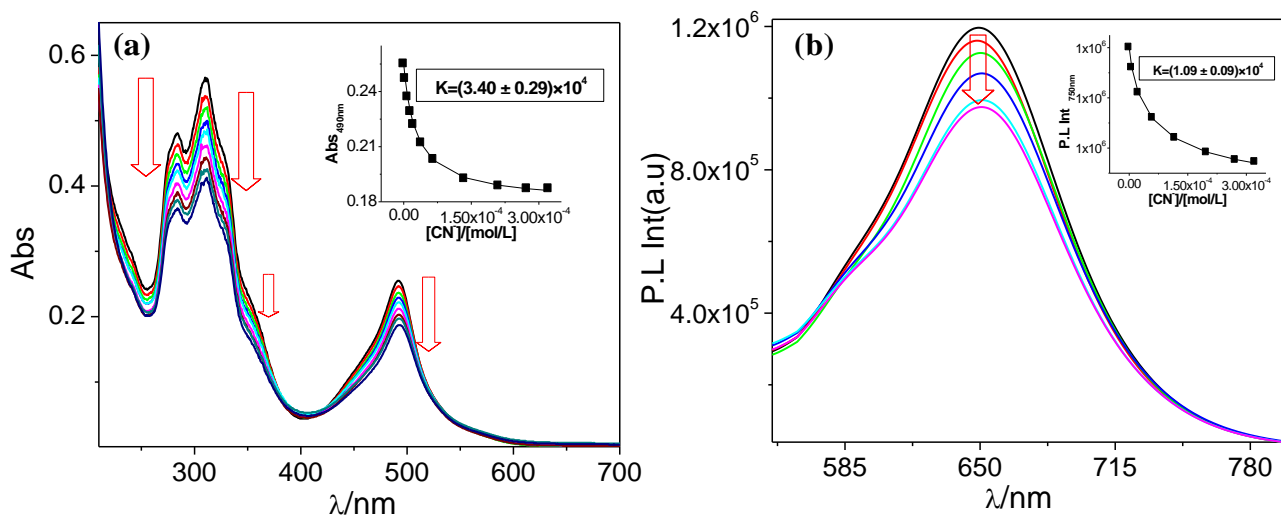


Figure S18. Changes in UV-vis absorption (a) and emission ($\lambda_{\text{ex}} = 490 \text{ nm}$) spectra (b) of **1** in aqueous solution upon incremental addition of CN^- ion. The insets show the change of absorbance and emission with equivalent of CN^- ion.

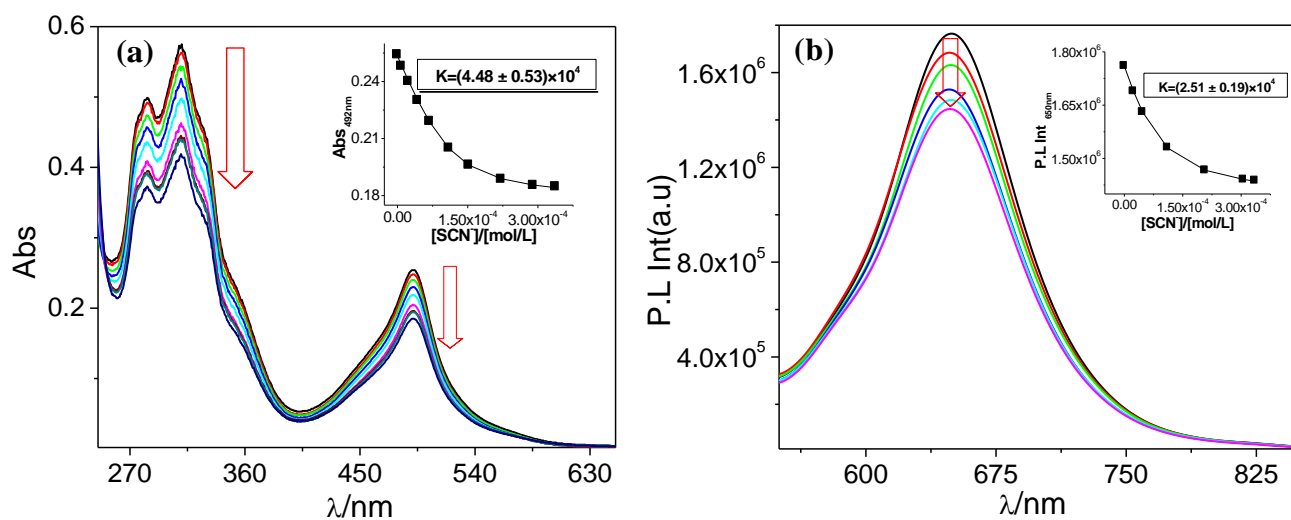


Figure S19. Changes in UV-vis absorption (a) and emission ($\lambda_{\text{ex}} = 490 \text{ nm}$) spectra (b) of **1** in aqueous solution upon incremental addition of SCN^- ion. The insets show the change of absorbance and emission with equivalent of SCN^- ion.

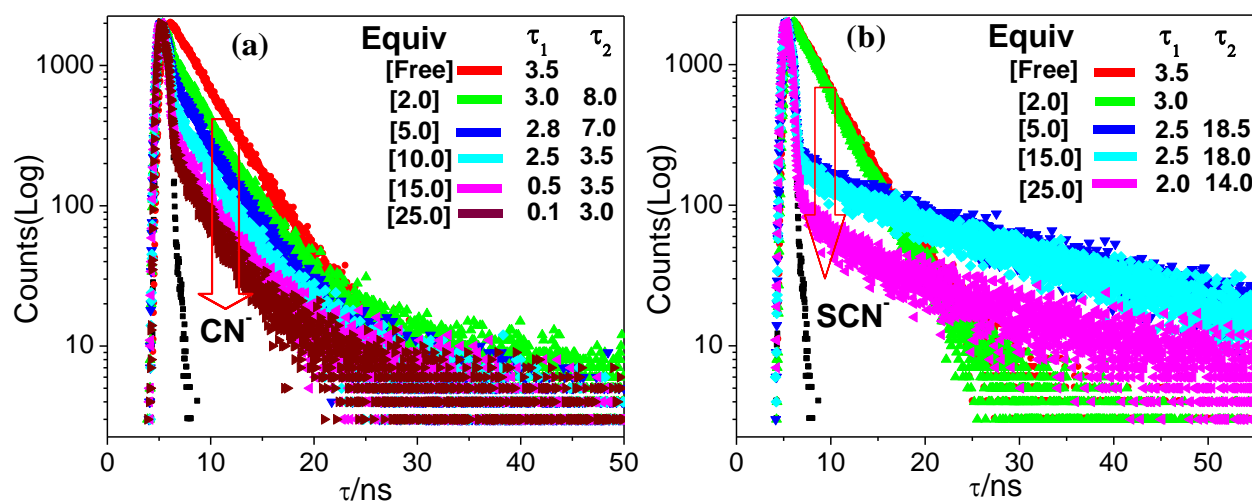


Figure S20. Change in luminescence decay ($\lambda_{\text{ex}} = 450 \text{ nm}$) profiles of **1** (a and b) in aqueous solution at room temperature upon incremental addition of CN^- and SCN^- , respectively. Insets show the lifetimes of the complex.

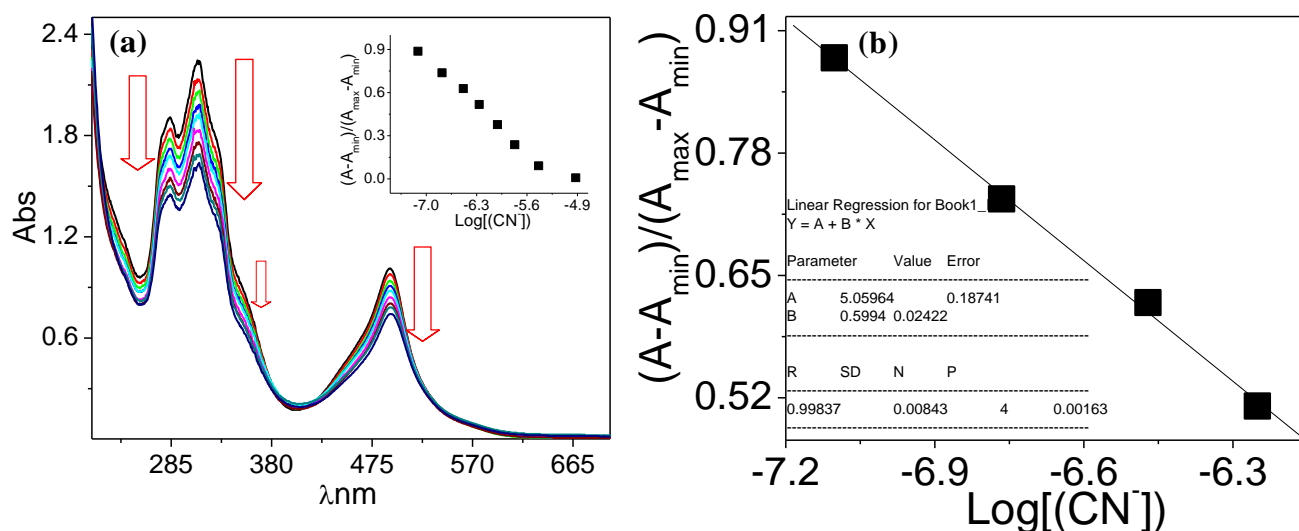


Figure S21. (a) Absorption spectral changes during the titration of the receptor **1** (2.0×10^{-5} M) with CN^- in aqueous solution, inset: Normalized absorbance between the minimum absorbance and the maximum absorbance. (b) A plot of $(A - A_{\min}) / (A_{\max} - A_{\min})$ vs $\text{Log}([\text{CN}^-])$, the calculated detection limit of receptor is 6.6×10^{-8} M.

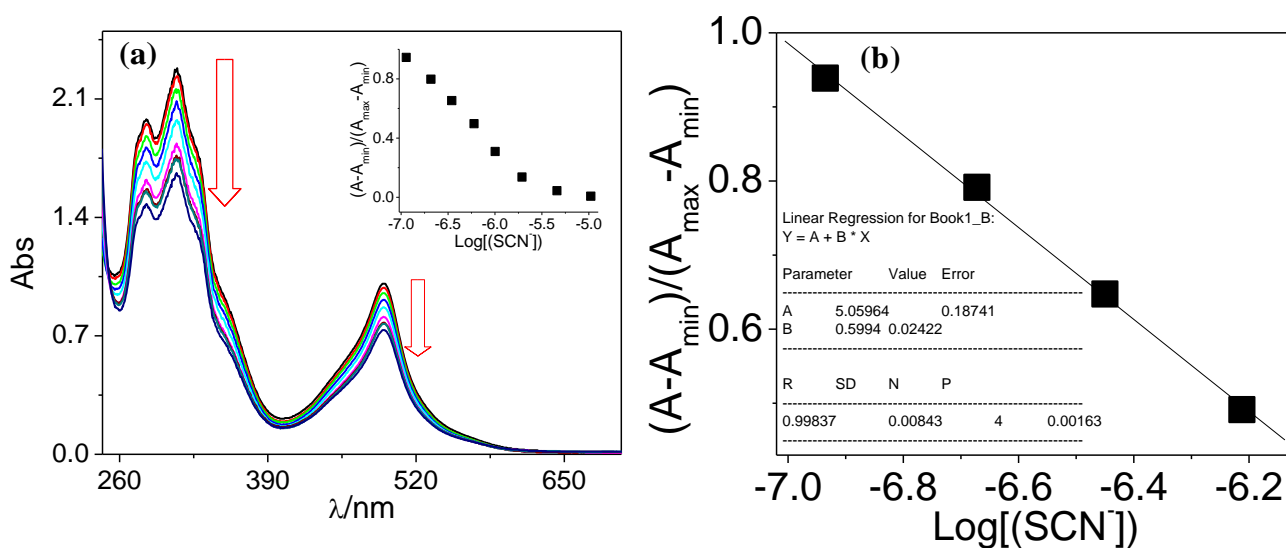


Figure S22. (a) Absorption spectral changes during the titration of the receptor **1** (2.0×10^{-5} M) with SCN^- in aqueous solution, inset: Normalized absorbance between the minimum absorbance and the maximum absorbance. (b) A plot of $(A - A_{\min}) / (A_{\max} - A_{\min})$ vs $\text{Log}([\text{SCN}^-])$, the calculated detection limit of receptor is 9.8×10^{-8} M.

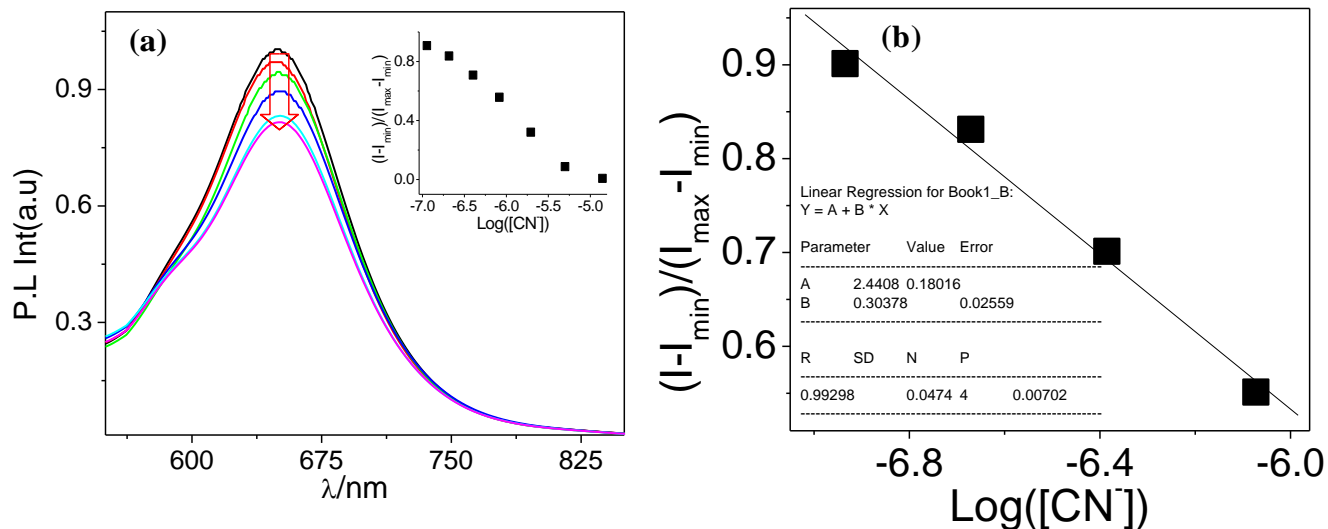


Figure S23. (a) Emission ($\lambda_{\text{ex}} = 490 \text{ nm}$) spectral changes during the titration of the receptor **1** ($2.0 \times 10^{-5} \text{ M}$) with CN^- in aqueous medium, inset: Normalized intensity between the minimum intensity and the maximum intensity. (b) A plot of $(I_{\text{min}})/(I_{\text{max}}-I_{\text{min}})$ vs $\text{Log}([\text{CN}^-])$, the calculated detection limit of receptor is $9.5 \times 10^{-8} \text{ M}$.

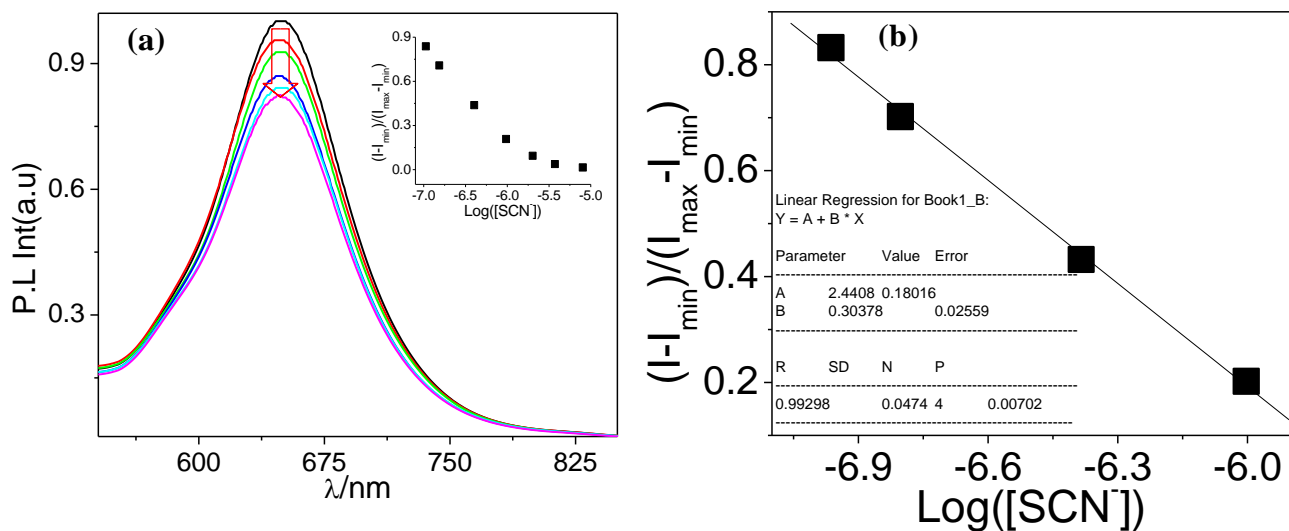


Figure S24. (a) Emission ($\lambda_{\text{ex}} = 490 \text{ nm}$) spectral changes during the titration of the receptor **1** ($2.0 \times 10^{-5} \text{ M}$) with SCN^- in aqueous medium, inset: Normalized intensity between the minimum intensity and the maximum intensity. (b) A plot of $(I_{\text{min}})/(I_{\text{max}}-I_{\text{min}})$ vs $\text{Log}([\text{SCN}^-])$, the calculated detection limit of receptor is $8.7 \times 10^{-8} \text{ M}$.

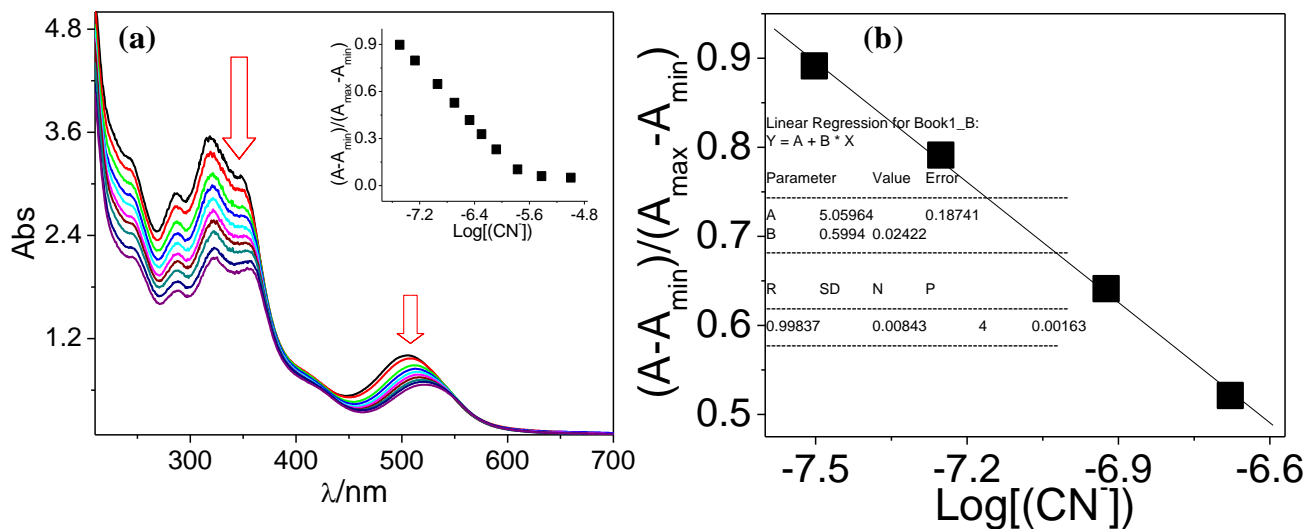


Figure S25. (a) Absorption spectral changes during the titration of the receptor **2** (2.0×10^{-5} M) with CN^- in aqueous solution, inset: Normalized absorbance between the minimum absorbance and the maximum absorbance. (b) A plot of $(A-A_{\min})/(A_{\max}-A_{\min})$ vs $\text{Log}([\text{CN}^-])$, the calculated detection limit of receptor is 2.6×10^{-8} M.

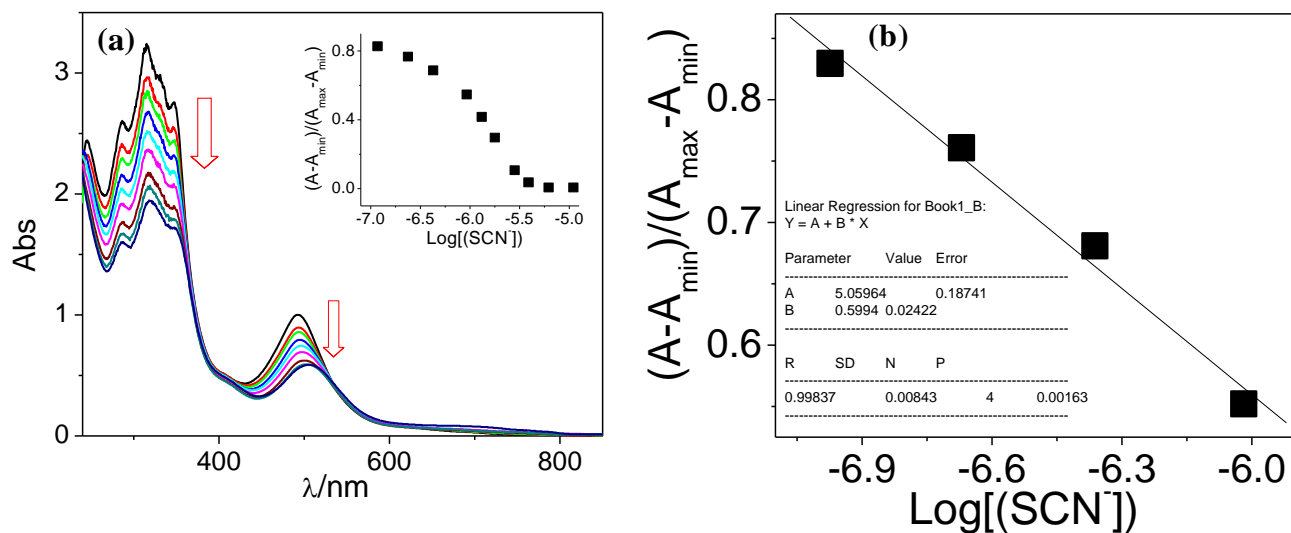


Figure S26. (a) Absorption spectral changes during the titration of the receptor **2** (2.0×10^{-5} M) with SCN^- in aqueous solution, inset: Normalized absorbance between the minimum absorbance and the maximum absorbance. (b) A plot of $(A-A_{\min})/(A_{\max}-A_{\min})$ vs $\text{Log}([\text{SCN}^-])$, the calculated detection limit of receptor is 8.5×10^{-8} M.

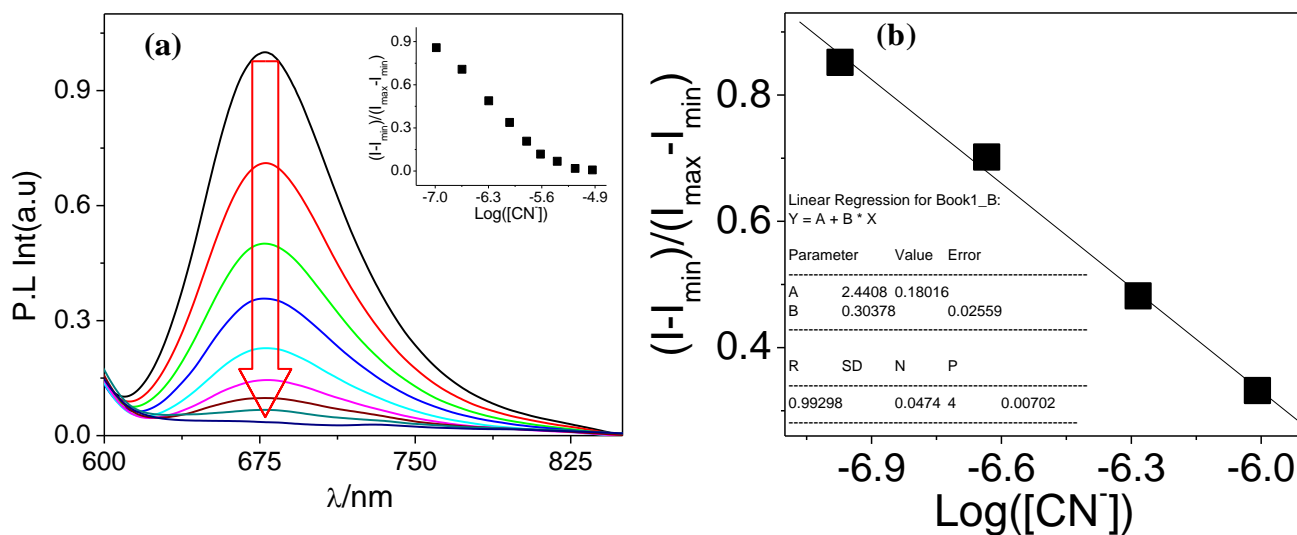


Figure S27. (a) Emission ($\lambda_{\text{ex}} = 490 \text{ nm}$) spectral changes during the titration of the receptor **2** ($2.0 \times 10^{-5} \text{ M}$) with CN^- in aqueous medium, inset: Normalized intensity between the minimum intensity and the maximum intensity. (b) A plot of $(I-I_{\text{min}})/(I_{\text{max}}-I_{\text{min}})$ vs $\text{Log}([\text{CN}^-])$, the calculated detection limit of receptor is $8.7 \times 10^{-8} \text{ M}$.

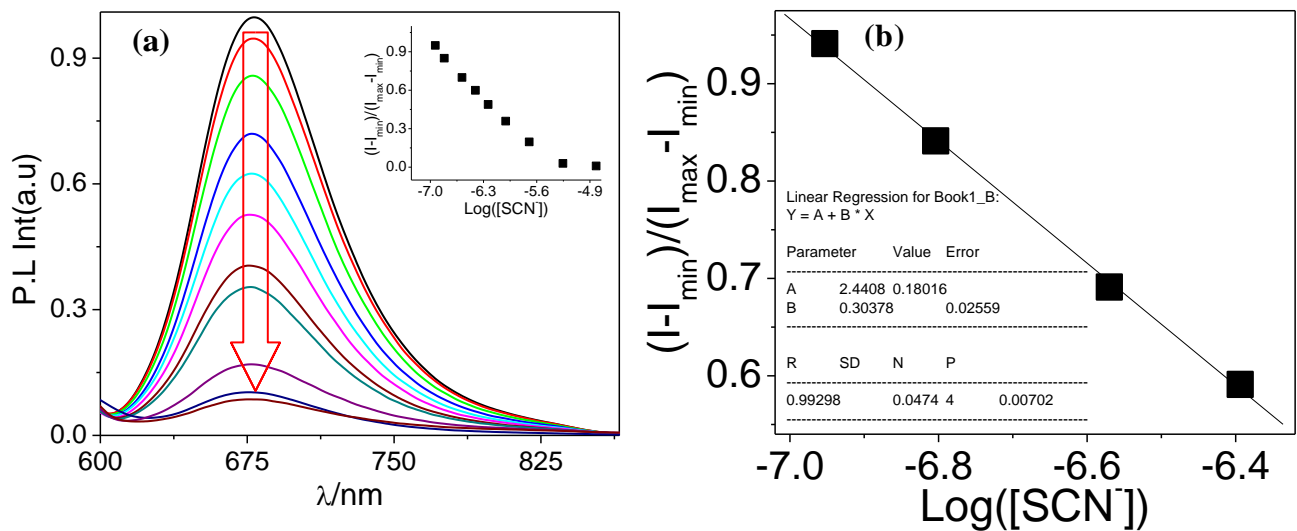


Figure S28. (a) Emission ($\lambda_{\text{ex}} = 490 \text{ nm}$) spectral changes during the titration of the receptor **2** ($2.0 \times 10^{-5} \text{ M}$) with SCN^- in aqueous medium, inset: Normalized intensity between the minimum intensity and the maximum intensity. (b) A plot of $(I-I_{\text{min}})/(I_{\text{max}}-I_{\text{min}})$ vs $\text{Log}([\text{SCN}^-])$, the calculated detection limit of receptor is $9.8 \times 10^{-8} \text{ M}$.

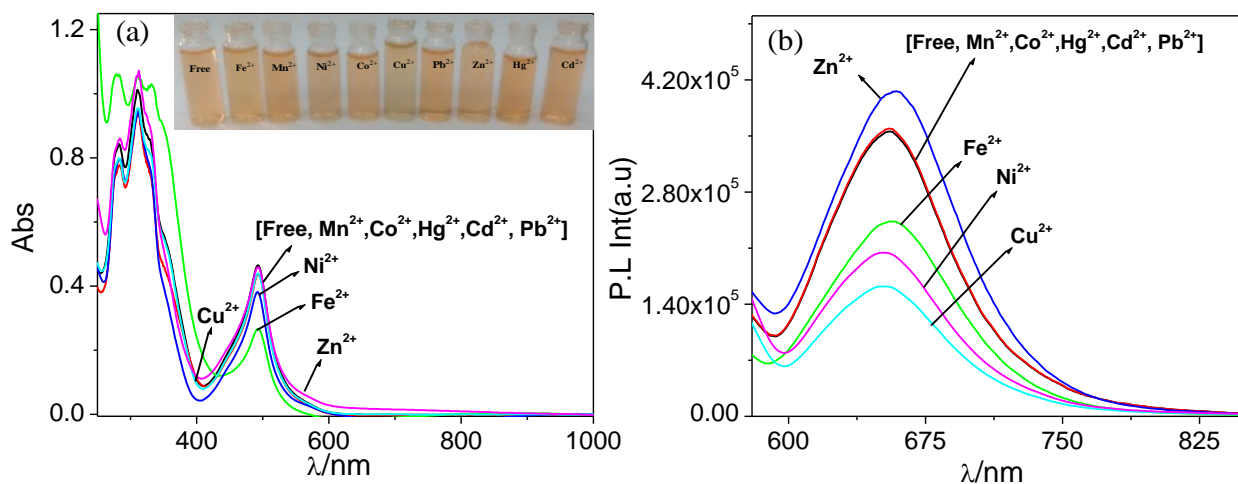


Figure S29. UV-vis absorption and emission ($\lambda_{\text{ex}} = 490 \text{ nm}$) spectral changes of **1** (a and b, respectively) in MeCN upon addition of different cations. The visual color changes upon addition of different cations are shown in the insets of Figure (a).

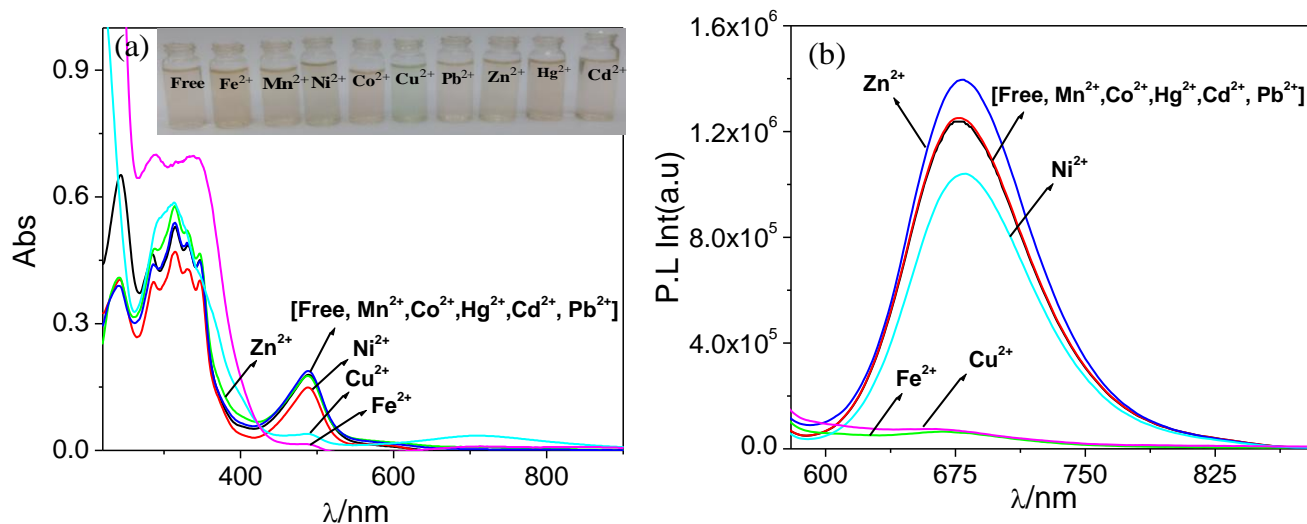


Figure S30. UV-vis absorption and emission ($\lambda_{\text{ex}} = 490 \text{ nm}$) spectral changes of **2** (a and b, respectively) in MeCN upon addition of different cations. The visual color changes upon addition of different cations are shown in the insets of Figure (a).

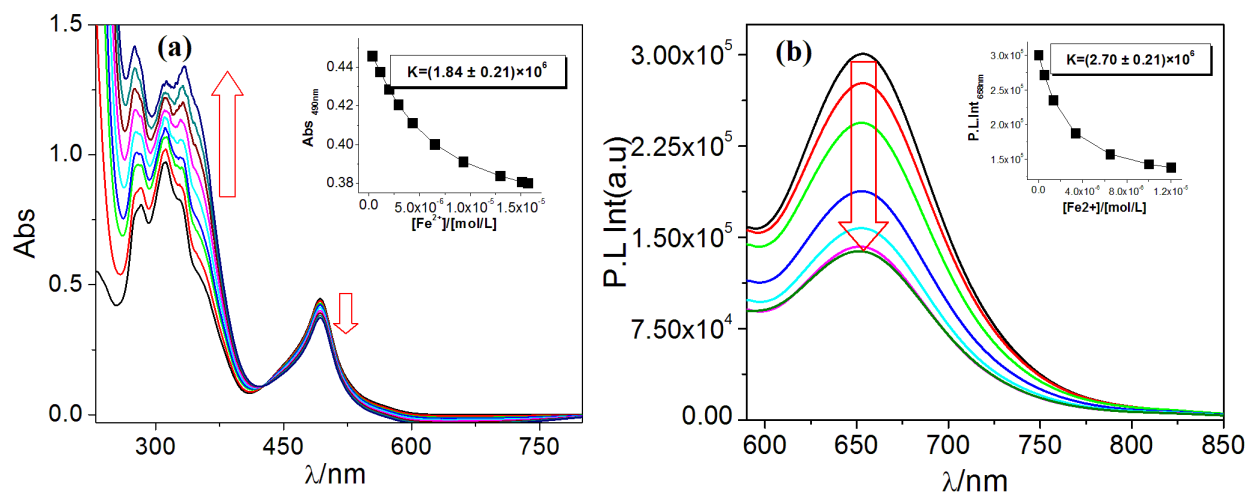


Figure S31. UV-vis absorption (a) and emission ($\lambda_{\text{ex}} = 490 \text{ nm}$) (b) spectral changes of **1** in MeCN upon addition of Fe^{2+} . The insets show the fit of the experimental absorbance and luminescence data to a 1:2 binding profile.

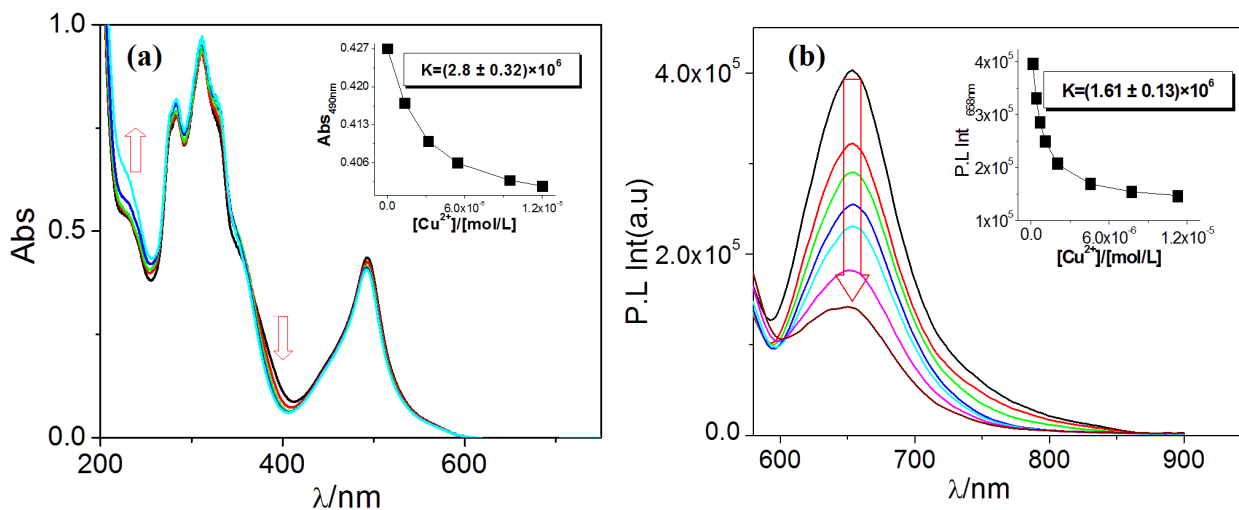


Figure S32. UV-vis absorption (a) and emission ($\lambda_{\text{ex}} = 490 \text{ nm}$) (b) spectral changes of **1** in MeCN upon addition of Cu^{2+} . The insets show the fit of the experimental absorbance and luminescence data to a 1:2 binding profile.

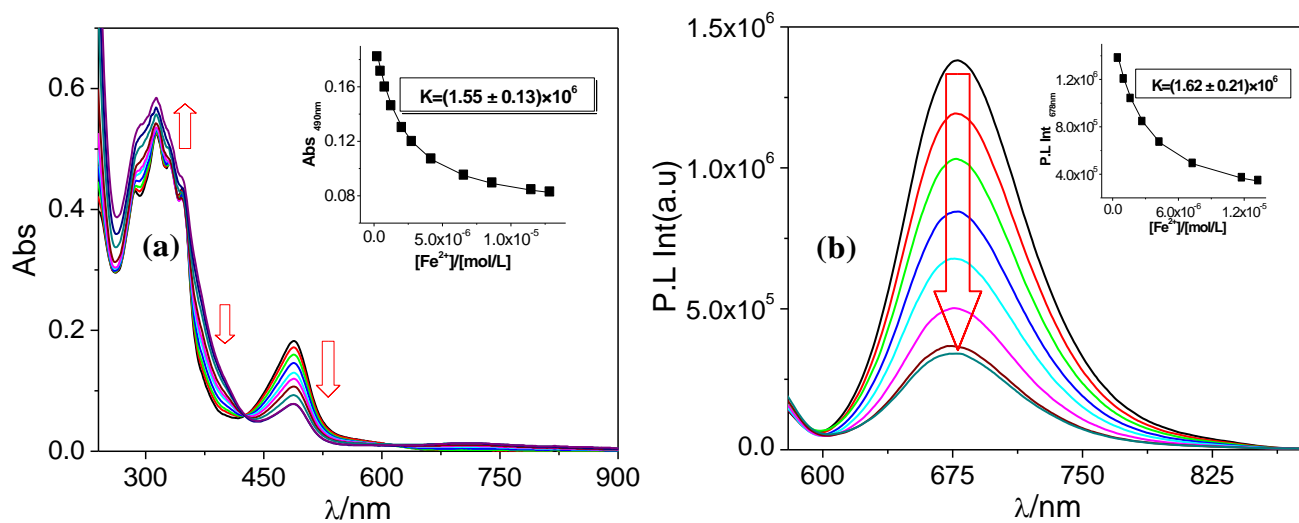


Figure S33. UV-vis absorption (a) and emission ($\lambda_{\text{ex}} = 490 \text{ nm}$) (b) spectral changes of **2** in MeCN upon addition of Fe^{2+} . The insets show the fit of the experimental absorbance and luminescence data to a 1:2 binding profile.

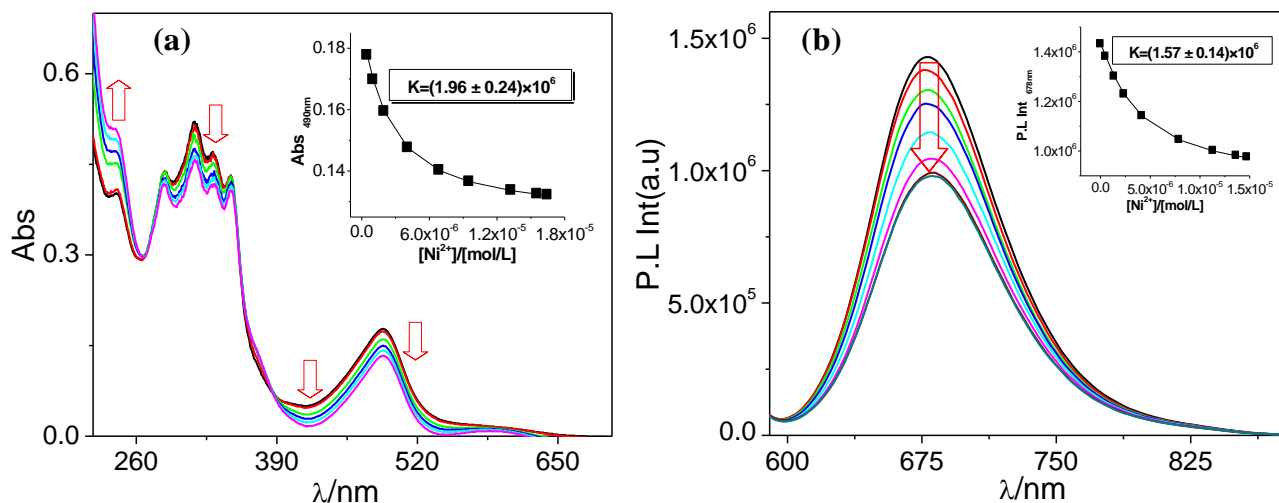


Figure S34. UV-vis absorption (a) and emission ($\lambda_{\text{ex}} = 490 \text{ nm}$) (b) spectral changes of **2** in MeCN upon addition of Ni^{2+} . The insets show the fit of the experimental absorbance and luminescence data to a 1:2 binding profile.

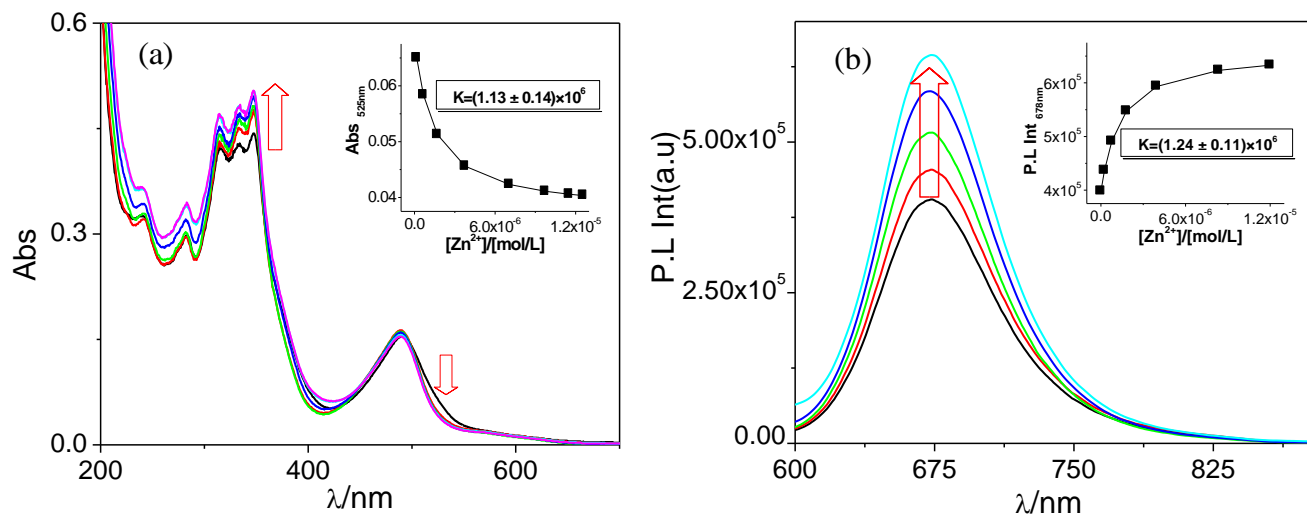


Figure S35. UV-vis absorption (a) and emission ($\lambda_{\text{ex}} = 490 \text{ nm}$) (b) spectral changes of **2** in MeCN upon addition of Zn^{2+} . The insets show the fit of the experimental absorbance and luminescence data to a 1:2 binding profile.

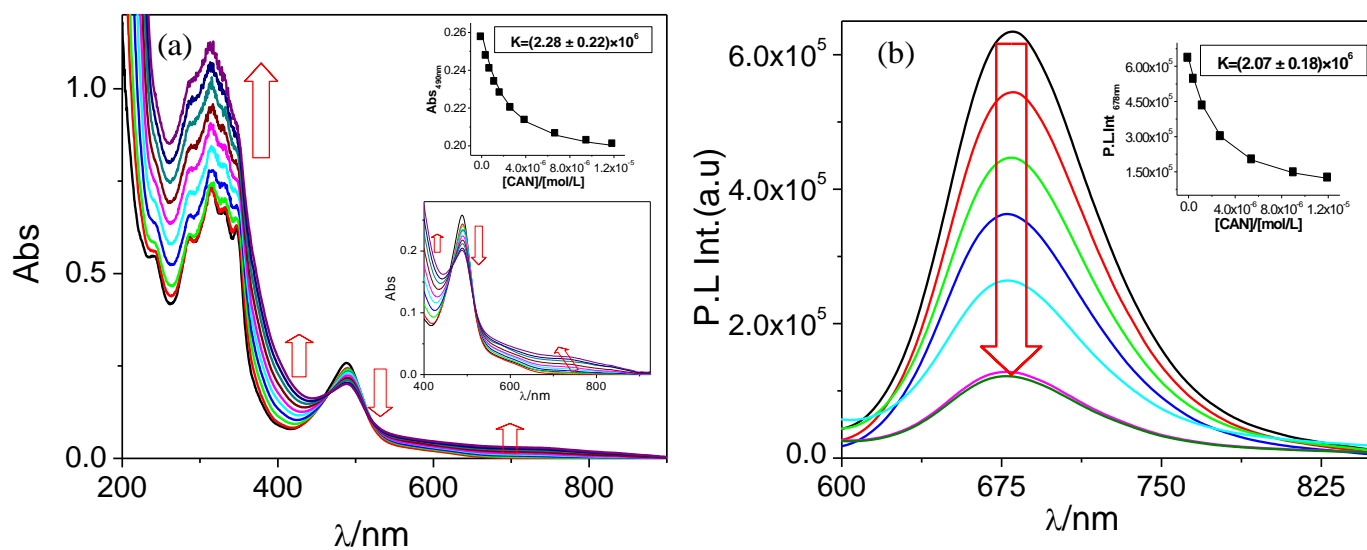


Figure S36. UV-vis absorption (a) and emission ($\lambda_{\text{ex}} = 490 \text{ nm}$) (b) spectral changes of **2** in MeCN upon addition of ceric ammonium nitrate (CAN). The insets show the fit of the experimental absorbance and luminescence data to a 1:2 binding profile.

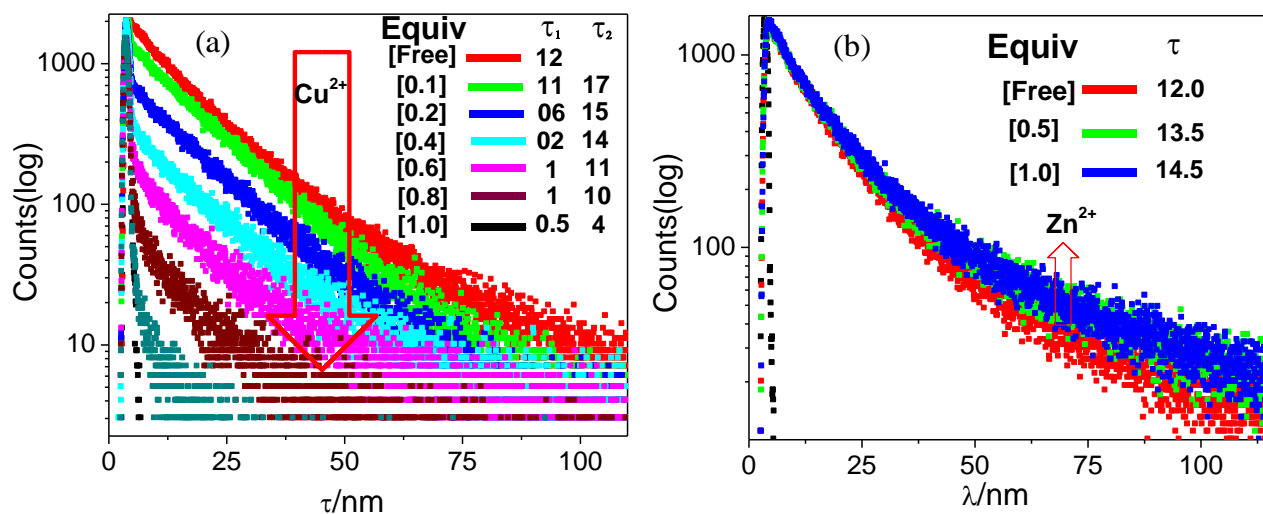


Figure S37. Change in time-resolved luminescence decay ($\lambda_{\text{ex}} = 450 \text{ nm}$) of **2** in MeCN at room temperature upon incremental addition of Cu^{2+} (a) and Zn^{2+} (b). Insets show the lifetimes.

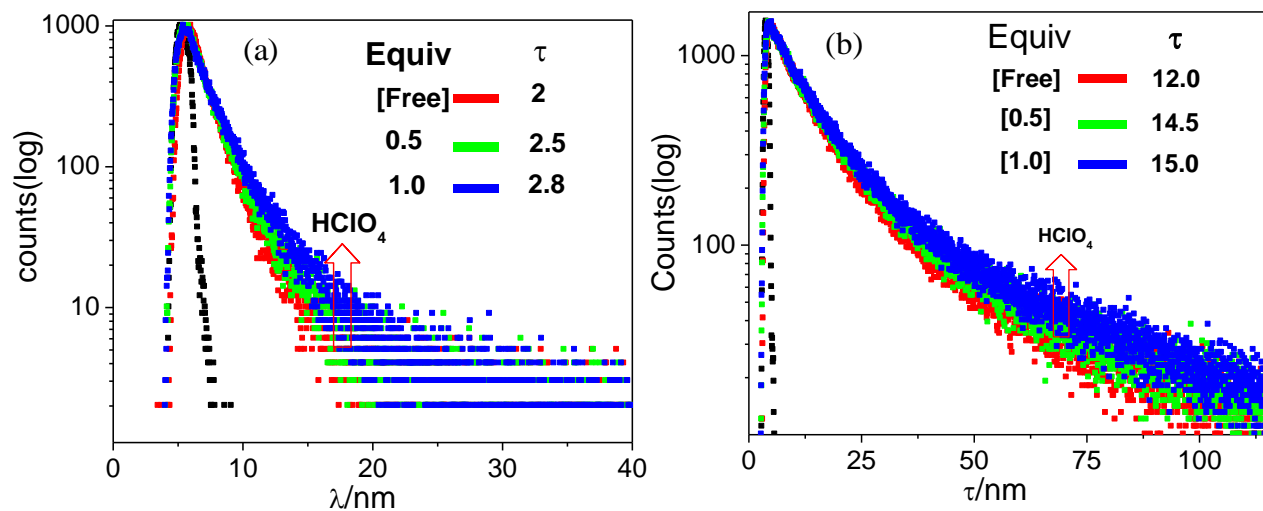


Figure S38. Change in time-resolved luminescence decay ($\lambda_{\text{ex}} = 450 \text{ nm}$) of **1**(a) and **2**(b) in acetonitrile solution at room temperature upon incremental addition of HClO_4 . Insets show the lifetimes of the complex.

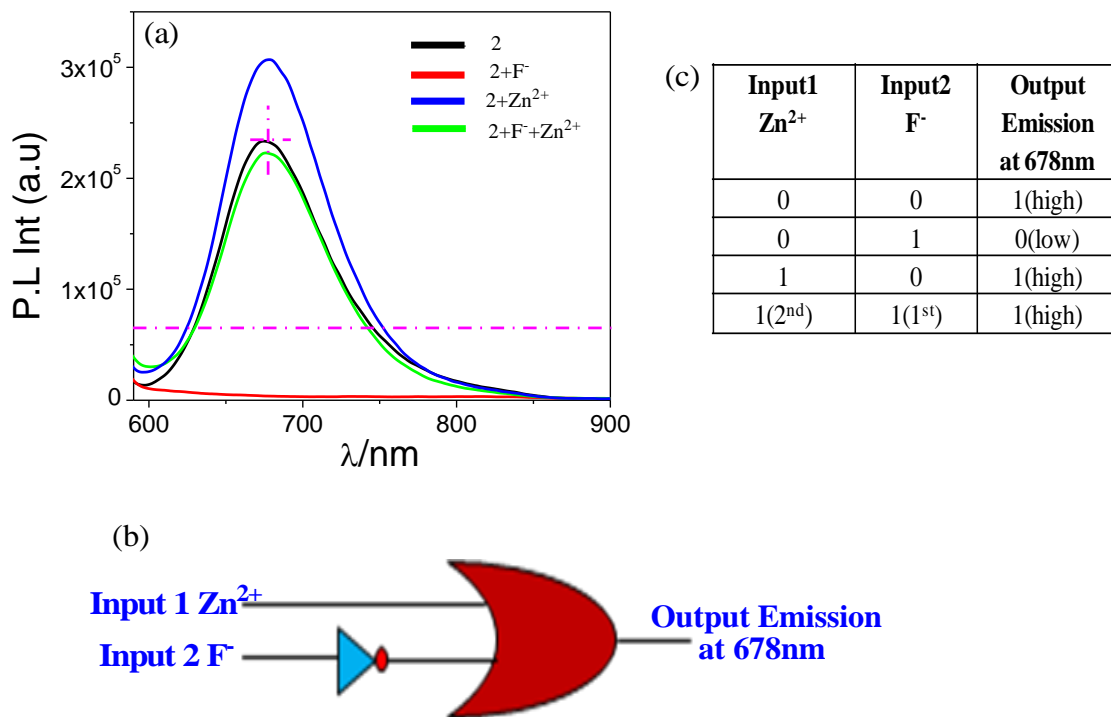


Figure S39. (a) Emission spectral changes of **2** upon the action of Zn²⁺ (input 1) and F⁻ (input 2). (b) Schematic representation of an IMPLICATION gate based on the emission at 678 nm, and (c) Corresponding Truth Table.

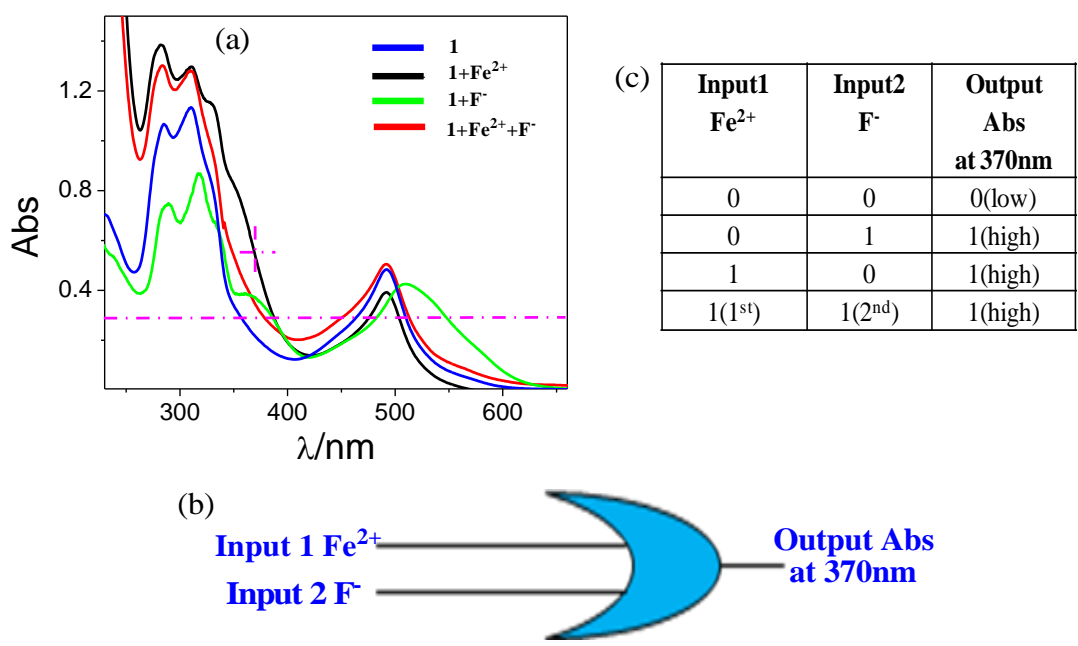


Figure S40. (a) Absorption spectral changes of **1** upon the action of Fe^{2+} (input 1) and F^- (input 2). (b) Schematic representation of an OR gate based on the absorption at 370 nm, and (c) Corresponding Truth Table.